ADVANCED ENERGY MATERIALS
www.advenergymat.de

Enabling Uniform and Accurate Control of Cycling Pressure for All-Solid-State Batteries

Yu-Ting Chen, Jihyun Jang, Jin An Sam Oh, So-Yeon Ham, Hedi Yang, Dong-Ju Lee, Marta Vicencio, Jeong Beom Lee, Darren H. S. Tan, Mehdi Chouchane, Ashley Cronk, Min-Sang Song, Yijie Yin, Jianting Qian, Zheng Chen, and Ying Shirley Meng**

All-solid-state batteries are emerging as potential successors in energy storage technologies due to their increased safety, stemming from replacing organic liquid electrolytes in conventional Li-ion batteries with less flammable solid-state electrolytes. However, all-solid-state batteries require precise control over cycling pressure to maintain effective interfacial contacts between materials. Traditional uniaxial cell holders, often used in battery research, face challenges in accommodating electrode volume changes, providing uniform pressure distribution, and maintaining consistent pressure over time. This study introduces isostatic pouch cell holders utilizing air as pressurizing media to achieve uniform and accurately regulated cycling pressure. $LiNi_{0.8}Co_{0.1}Mn_{0.1}O_2$ | Li_6PS_5Cl | Si pouch cells are fabricated and tested under 1 to 5 MPa pressures, revealing improved electrochemical performance with higher cycling pressures, with 2 MPa as the minimum for optimal operation. A bilayer pouch cell with a theoretical capacity of 100 mAh, cycled with an isostatic pouch cell holder, demonstrated a first-cycle Coulombic efficiency of 76.9% and a discharge capacity of 173.6 mAh g^{-1} (88.1 mAh), maintaining 83.6% capacity after 100 cycles. These findings underscore the effectiveness of isostatic pouch cell holders in enhancing the performance and practical application of all-solid-state batteries.

1. Main Text

All-solid-state batteries (ASSBs) are hailed as one of the next-generation energy storage technologies and tremendous efforts have been invested to their development. As solid-state electrolytes (SSEs) are employed to replace liquid electrolytes in conventional Li batteries, ASSBs exhibit reduced flammability and leakage issues.[1–4] Moreover, anodes with high specific capacity, such as pure Si,[5,6] have been reported to achieve long cycle life in ASSBs, but meets challenges in liquid electrolytes as Si will suffer from pulverization during cycling resulting in continuous solid electrolyte interphase (SEI) formation.[7–11] Despite these advantages, there are many engineering challenges for ASSBs stemming from solid-solid interfacial contacts.[12] The inability to flow and infiltrate into voids in the electrode is a double-edged sword: it limits the SEI formation, but

Y.-T. Chen, S.-Y. Ham, A. Cronk, Y. Yin, J. Qian, Z. Chen, Y. S. Meng
Program of Materials Science and Engineering
University of California San Diego
La Jolla, CA 92093, USA
E-mail: zhc199@ucsd.edu; shmeng@uchicago.edu

J. Jang, J. A. S. Oh, D.-J. Lee, M. Vicencio, D. H. S. Tan, Z. Chen, Y. S. Meng
Department of NanoEngineering
University of California San Diego
La Jolla, CA 92093, USA

The ORCID identification number(s) for the author(s) of this article can be found under https://doi.org/10.1002/aenm.202304327

DOI: 10.1002/aenm.202304327

J. Jang
Department of Chemistry
Sogang University
35 Baekbeom-ro, Mapo-Gu, Seoul 04107, South Korea

H. Yang, M. Chouchane, Y. S. Meng
Pritzker School of Molecular Engineering
The University of Chicago
Chicago, IL 60637, USA

J. B. Lee, M.-S. Song
LG Energy Solution, Ltd.
LG Science Park
Magokjungang 10-ro, Gangseo-gu, Seoul 07796, South Korea

Z. Chen, Y. S. Meng
Sustainable Power & Energy Center (SPEC)
University of California San Diego
La Jolla, CA 92093, USA

Z. Chen
Program of Chemical Engineering
University of California San Diego
La Jolla, CA 92093, USA

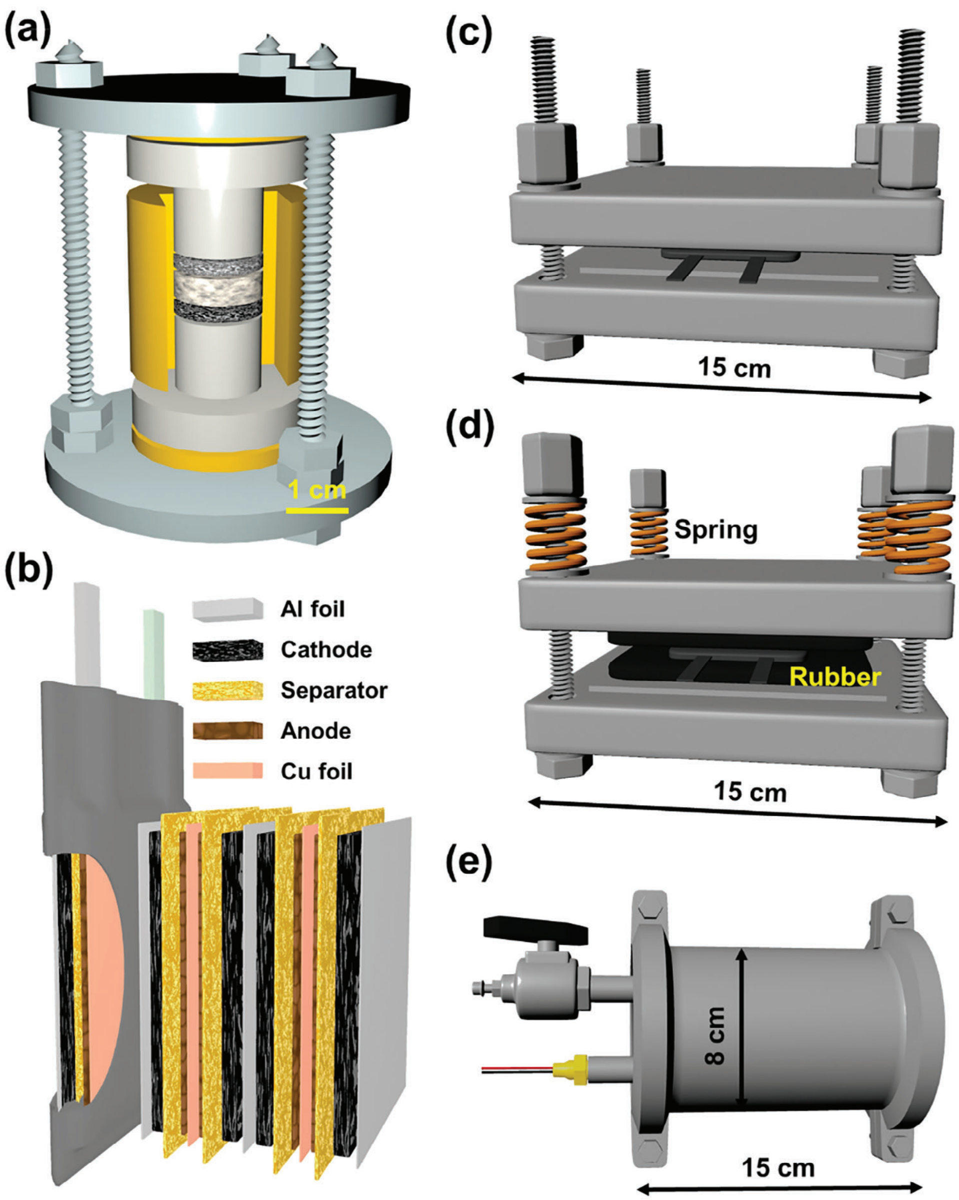

Figure 1. The structure of a) a plunger cell clamped in a cell holder, and b) a multilayer pouch cell. The schematic of c) a bare UPCH with simple metal plates, d) an improved UPCH with springs and rubber gaskets, and e) an IPCH.

volumetric changes in the electrode can potentially cause detachment of electrode material – SSE interfaces.[13,14] This leads to deteriorating electrochemical reaction in the ASSBs. As such, pressure becomes a crucial factor to maintain intimate interfacial contact and ensure the performance of ASSBs – not only in cell fabrication, but also during cell cycling.

Pellet-type ASSBs are usually employed in research labs for electrochemical tests. A polymer die and a pair of metal plungers are employed to contain and apply fabrication pressure to pelletize the materials. During electrochemical tests, a cell holder consisting of bolts, nuts, and plates is required to apply cycling pressure and the metal plungers serve as current collectors (**Figure** 1a). As most inorganic SSEs are brittle, SSE layers typically have a high thickness of ≈500 µm to guarantee a sufficient strength to support the cells mechanically. This reduces the energy density of ASSBs, as SSE layers do not store energy.[15–18] Moreover, due to the friction at the die walls during uniaxial compaction and the parallelism tolerance at the metal plungers, it is challenging to achieve a uniform density distribution throughout the whole pellet.[19] Furthermore, voids tend to form on the cathode-SSE interfaces in the non-pressurization direction when volume changes of cathodes occur during cycling, and these may negatively affect their electrochemical performance.[19,20] By having smaller layer thickness, larger electrode area, and no requirement of polymer dies, pouch cells not only exhibit significantly higher energy density, but also achieve better density distribution after calendering (Figure 1b). As the wrapping materials of pouch

Table 1. The formats and the cycling conditions of ASSPC reported in the literature and our work.

Ref	Cathode | SSE | Anode	Temperature [°C]	Fabrication pressure [MPa]	Cycling Pressure [MPa]	cycle number	areal capacity [mAh cm^{-2}]	C rate	Dimension [cm^2]
[35]	$LiNi_{0.8}Co_{0.15}Al_{0.05}O_2$ | $Li_2SeP_2S_5$ | Graphite	25			100	4.2	0.1 C	8.8 × 5.3
[36]	$LiNi_{1/3}Co_{1/3}Mn_{1/3}O_2$ | 75 Li_2S·25 P_2S_5 | Graphite	30	330 MPa		10	1.536	C/24	2 × 2
[37]	$LiNi_{0.6}Co_{0.2}Mn_{0.2}O_2$ | Li_6PS_5Cl | Graphite	30	492 MPa			4.2	0.025 C	8 × 6
[21]	$LiNi_{0.8}Co_{0.1}Mn_{0.1}O_2$ | Li_6PS_5Cl | C-Ag	60	490 MPa	2	1000	6.8	0.5 C	11.2 × 6.7
[5]	$LiNi_{09}Co_{0.05}Mn_{0.05}O_2$ | Li_6PS_5Cl | PVD-Si	25	300 MPa	20	50	3	0.05 C	2.5 × 2.5
[38]	S | Li_6PS_5Cl | Li	30	300 MPa		10	3	0.01 C	3 × 3
[17]	$LiNi_{0.8}Co_{0.1}Mn_{0.1}O_2$ | Li_6PS_5Cl | LiIn	25			200		0.15 C	6 × 6
[39]	Sulfur | Solid electrolyte | LiIn	30	500 MPa		50	3.2	0.05–2 C	
[40]	$LiNi_{0.6}Co_{0.2}Mn_{0.2}O_2$ | Li_6PS_5Cl | LiIn				100	4	0.1 C	
Our work	$LiNi_{0.8}Co_{0.1}Mn_{0.1}O_2$ | Li_6PS_5Cl | Si	30	500 MPa	5	100	4	0.2 C	Double 3.5 × 3

cells are flexible, isostatic pressure can be applied to further improve the density uniformity, which has been well-demonstrated in the literature.[19,21]

Although multiple groups have claimed to demonstrate solid-state pouch cells in the literature, many adulterate excess amount of polymer binders, Li salts, and even solvents to boost the performance.[16,17,22–30] These defeat the safety feature of ASSBs. Several all-solid-state pouch cells (ASSPC) with more than 3 mAh cm^{-2} employing only inorganic SSE (with low amounts of binders) were reported (**Table 1**), which is similar to or higher than that in commercial Li batteries. Nevertheless, many cells were tested at C-rates lower than 0.1 C, and elevated temperature was required to realize higher C-rates and areal capacities. As SSEs do not flow and conform to the shape of electrode materials like liquid electrolytes, a pressure must be applied to ASSBs to ensure intimate interfacial contact, both in fabrication and during cycling.[12,19,31] Most articles report only fabrication pressure, typically 300 to 500 MPa, without mentioning cycling pressure. However, cycling pressure is a more important metric for commercialization, as high cycling pressure will vastly increase the dead weight of the system and sacrifice the module energy density. Since a low cycling pressure usually results in insufficient interfacial contact, and thus worse electrochemical performance of ASSBs, it is critical to design cell holders that provide uniform cycling pressure.

Pouch cell holders consisting of bolts, nuts, and rigid plates are employed in most articles to apply uniaxial pressure to pouch cells (Figure 1c). Some may attach bearings between moving plates and bolts to ensure smooth movement and parallelism. However, several studies have observed that the cycling pressure of ASSBs changes during cell cycling due to the volume change of electrode materials.[32,33] For example, Si undergoes 300% of volume expansion and the thickness of Li metal anodes increases ≈5 µm when each mAh cm^{-2} is plated.[34] This may negatively affect their electrochemical performance, especially when pressure sensitive materials, such as Li metal, are used. To address this problem, Ham et al incorporated springs into the cell holders to accommodate cycling volume change. Such a design successfully reduced the cycling pressure change of a $LiNi_{0.8}Co_{0.1}Mn_{0.1}O_2$ (NCM811) | Li cell from 2 MPa to less than 0.5 MPa, and thus doubled its critical current density at 40 °C.[33] Inspired by this work, an improved uniaxial pouch cell holder (UPCH) design containing springs and rubber gaskets was also proposed (Figure 1d).[16] Nevertheless, rubber and springs may be susceptible to material fatigue and the applied force would decrease over time. It is noteworthy that the cell pressure may also change if the ambient temperature fluctuates, since the thermal expansion coefficients of pouch cells and bolts are different. As such, pressure regulation systems are required to ensure the stability of cell cycling. Unfortunately, regulating the pressure accurately by turning the bolts is challenging, as the motors need to overcome large friction under high pressure load, and extra effort is needed to synchronize the torque of the bolts in the cell holder. To tackle this issue, fluids, including gases and liquids, can potentially be utilized as pressurizing media to apply isostatic cycling pressure. Gases can be used when light weight, low cost, or low X-ray absorption (e.g., in-situ cell characterization applications) are needed, and liquids can be employed when pressure load and heat dissipation are demanding. Instead of bolts and nuts, an isostatic pouch cell holder (IPCH) requires a chamber and gaskets to contain the pressurized fluid and ASSPCs. A valve is installed to fill or evacuate the fluid, and a wire fit-through is implemented to electrically connect ASSPCs inside the chamber (Figure 1e). As fluids are significantly more compressible and conforming than solids, IPCHs can easily accommodate cell volume changes during cycling. Moreover, the pressure regulating systems of pressurized fluids and gases are mature and widely available, and thus maintaining a constant cycling pressure in IPCHs for an extended period of time can be easily achieved, even in an environment with large temperature fluctuation. To verify our

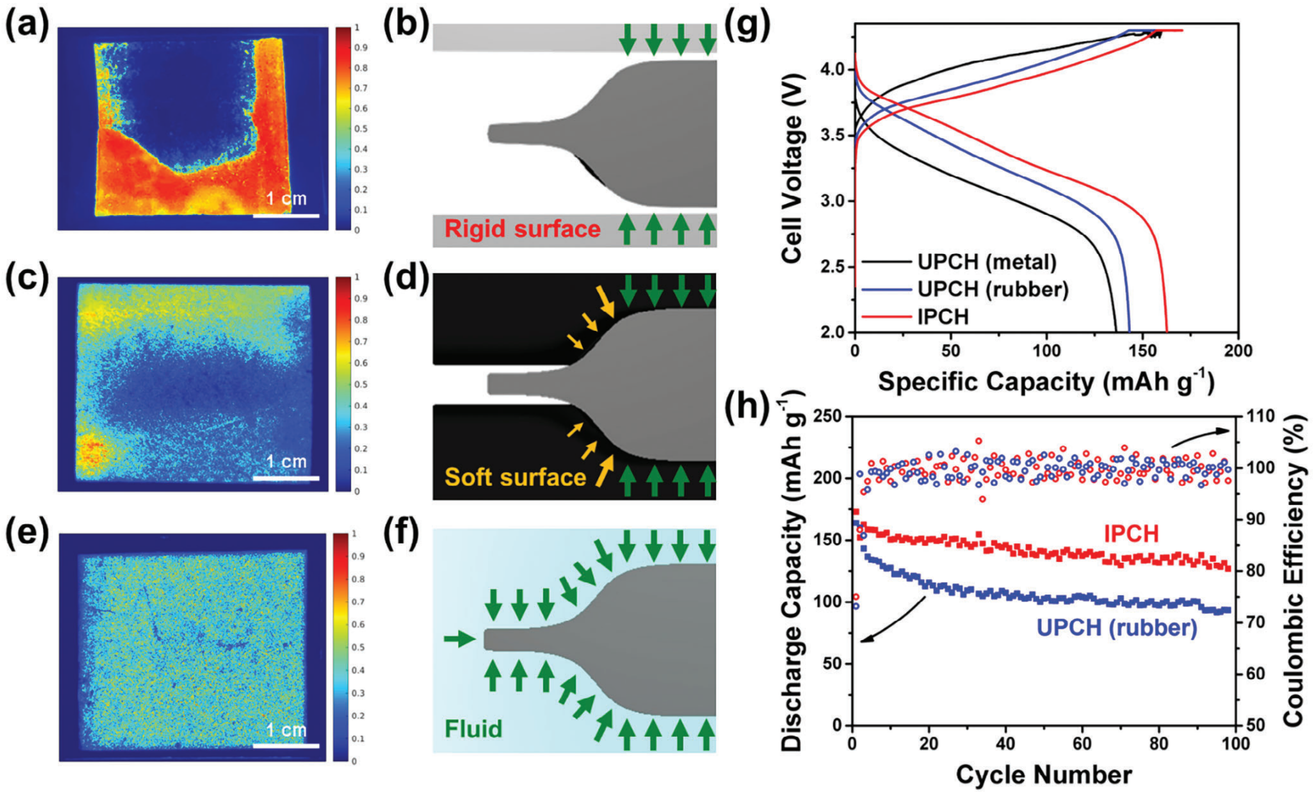

Figure 2. The experimental pressure paper observation and the schematics of the force distribution on the sealing edges of ASSPCs when a,b) uniaxial pressure is applied by rigid metal surfaces with a bare UPCH, c,d) uniaxial pressure is applied by soft rubber gaskets with an improved UPCH, and e,f) isostatic pressure is applied by fluids with an IPCH, respectively. g) The voltage profiles of first cycle and h) the reversible discharge capacity of ASSPCs when uniaxial and isostatic pressures were applied.

perspective, three cell holders, including a bare UPCH with rigid metal surfaces, an improved UPCH with rubber gaskets and springs, and IPCHs were assembled. The electrochemical performances were all tested with ASSPCs at 30 °C under cycling pressures from 5 to 1 MPa throughout the whole study. Compared to the past works, which still relied heavily on pellet type ASSBs under high cycling pressures for electrochemical tests, the new concept discussed in this study successfully reduced the demand for cycling pressure and temperature, while increased the energy density and maintained the electrochemical performance of ASSBs, pathing a way toward practical deployment of ASSBs.

2. Results and Discussion

The digital images of the bare UPCH and improved UPCH with springs and rubber gaskets are presented in Figure S1 (Supporting Information). To observe the pressure distribution at 5 MPa, pressure paper was sealed in pouch cases (without actual cell components) and placed in different cell holders. Upon receiving a pressure higher than its threshold, the pressure paper would turn red, and their digital images were taken (Figure S2, Supporting Information). To better visualize the pressure distribution, the digital images were converted to color gradient charts. An inhomogeneous pressure distribution was observed for the uniaxial set-up (**Figure** 2a; Figure S2a, Supporting Information). When a rigid surface (such as bare metal) is used to apply a uniaxial pressure, areas that are out of contact (e.g., the edges of ASSPCs or imperfect surface flatness of the metal plates forming concave regions) will experience a lower or no pressure. The pressure will concentrate on the rest of the area, resulting in overpressurization (Figure 2b,c). These problems were slightly mitigated with the improved UPCH, as rubber gaskets were able to conform to the shape of the metal plates and the ASSPC. Nevertheless, a uniform pressure distribution was still not observed (Figure 2c; Figure S2b, Supporting Information), as the degree of deformation of the rubber gaskets was lower at the areas with larger gaps, resulting in lower pressures (Figure 2d). To further improve the uniformity of the cycling pressure, an IPCH was designed, and its digital image and schematic figure are presented in Figure S3 (Supporting Information). The structure of an IPCH consists of a sealed chamber to confine the pressurized fluid and accommodate the ASSPC, a pressure gauge to monitor the chamber pressure, a wire fit-through to enable cycling of the ASSPC sealed in its chamber, and a ball valve able to connect to an air compressor to pressurize, or depressurize the compressed air. Air was selected as the pressurizing medium in this study because of its availability and low cost. Pressure paper was vacuum sealed into a pouch bag, pressurized with an IPCH and the pressure distribution is presented in Figure 2e and Figure S2c (Supporting Information). A uniform pressure distribution was observed. This can be explained by Pascal's principle, which states that a change in pressure applied at any point in the confined fluid at rest is transmitted undiminished throughout the fluid in all directions (Figure 2f).

To understand how pressure uniformity affect electrochemical performance, three NCM811 | Li_6PS_5Cl (LPSCl) | Si ASSPCs with a cathode size of 3.5 × 1.5 cm^2 and an areal capacity of 4 mAh cm^{-2} were assembled, calendered at 500 MPa (this cell format was used for the rest of the article), pressurized with the three pouch cell holders, and cycled under 5 MPa at ambient temperature. The cycling pressure of the UPCH was estimated by the torque values of bolts and nuts, and that of IPCH was by observing the pressure gauge. Figure 2g shows voltage profiles of their first cycle. The cell had a soft short during charging if the uniaxial pressure was applied with rigid metal surfaces (bare UPCH), possibly due to having the worst pressure uniformity causing inhomogeneous Li flux in the system. The ASSPCs cycled with the improved UPCH and the IPCH successfully reached 100 cycles (Figure 2h). As IPCH provides better pressure uniformity and is less susceptible to structural fatigue (which may lead to cycling pressure drop over time), it exhibited a capacity retention of 126.8 mAh g^{-1} after 100 cycles, higher than that of the improved UPCH (93.5 mAh g^{-1}).

Other than superior electrochemical performance, IPCHs can possibly provide higher energy density than UPCHs at the module level due to the reduced demand of the structural components. There are two physical limitations that IPCHs can avoid: having limited number of cells in a cell stack (Figure S4a, Supporting Information) and flexing of the pressurizing plates. When a UPCH is used (Figure S4b, Supporting Information), pressure is transmitted through other ASSPCs. As such, all ASSPCs, including all layers inside every single pouch, must be perfectly aligned, which becomes more challenging and costly as the number of cells in one stack increases. The plates must also be sufficiently thick to resist bending, which may result in applying higher pressure to the edges and lower pressure to the centers of ASSPCs (Figure S4c, Supporting Information). As fluid is employed as pressurizing media in an IPCH, pressure is identically applied to all points in all directions. Hence, deformation of the vessel wall and arrangement of ASSPCs will not affect the pressure uniformity. As a result, thinner walls can be used in IPCHs to reduce module weight. The estimated required weights of UPCHs and IPCHs using different metal alloys with a pressure rating from 1 to 10 MPa are presented in Figure S5 (Supporting Information). IPCHs are all hypothetically lighter than UPCHs. The weights of IPCHs can be further reduced if polymers and composite materials (which often exhibit high tensile strength but low Young's modulus) are employed. Implementing ASSPC formats with higher energy density, such as jelly roll and Z-stacking, gives IPCHs a further edge, as there are fewer shape limitations for IPCHs. The details for holder weight estimations are discussed in Note S1 (Supporting Information).

Taking advantage of accurate pressure control and uniform pressure distribution, the effect of cycling pressure of the IPCHs were further evaluated at 30 °C to avoid the fluctuation of ambient temperature. It is worthy to note that the ASSPCs were activated at 5 MPa, and reduced to the target cycling pressures, ranging from 5 to 1 MPa (**Figure 3**a, and the Coulombic efficiency plots are shown in Figure S6, Supporting Information). At 0.1 C, cells cycled at all pressures except 1 MPa exhibited a similar discharge capacity of ≈160 mAh g^{-1}, and the slight difference was due to batch variance of cathode composites. A minimum cycling pressure of 2 MPa was required to keep a good interfacial contact in the ASSPCs assembled in this study. The effect of cycling pressure became evident when the C-rate was above 0.3 C. At 1 C, the polarization of the cell grew so drastically that only 30 mAh g^{-1} could be obtained with a cycling pressure of 5 MPa. Nevertheless, ASSPCs cycled above 2 MPa regained most of their discharge capacities when the C-rate decreased back to 0.1 C. Pressures of 5, 3, and 2 MPa, were selected to conduct the long cycling test (Figure 3b), and were cycled at a moderate rate of 0.2 C to distinguish the effect of cycling pressure to capacity retention while not vastly deteriorating the discharge capacities according to the rate capability test. As the cycling pressure decreased, it required more cycles for the Coulombic efficiency to reach near 100%, and the initial discharge capacity decreased from 149.7 mAh g^{-1} at 5 MPa to 135.4 mAh g^{-1} at 2 MPa. Reduced Coulombic efficiency and faster capacity fade at lower cycling pressures could be attributed to more unwanted surface reactions and more severe delamination on the cathode-SSE interfaces, which resulted in worse ionic conductive pathways.[41,42] The capacity retention after 100 cycles also deteriorated from 77.8% at 5 MPa to 47.7% at 2 MPa, due to loss of interface contact. As electrode materials underwent repetitive volume change, it is crucial to apply pressure to maintain physical contact between SSE and electrode materials, and a higher pressure tends to support intimate interfacial contact. The electrochemical impedance spectroscopy (EIS) of 1st and 100th cycle of the three ASSPCs (Figure S7 and Table S1, Supporting Information) were fitted (Figure 3c). Four components were used in the model: the bulk, grain boundary of SSE, charge transfer of anode, and cathode.[43–45] The charge transfer of cathode and anode were combined in the first cycle, as their time constants highly overlapped and could not be deconvoluted. All ASSPCs exhibited very similar SSE impedance values at different cycling pressures and cycle numbers, indicating that SSE separator layers were stable during cycling and not sensitive to cycling pressure. Interestingly, an extra semicircle at mid-frequency appeared after 100 cycles. To accurately identify the impedance components, a three-electrode ASSPC, consisting of NCM811 cathode, Si anode and Li metal as the working, counter and reference electrodes, respectively, was assembled (Figure 3d; Figure S8a, Supporting Information).[46] The EIS of cathode, anode and full cell were measured when the cell was discharged to 3.4 V in each cycle. After 10 cycles at 5 MPa, the Nyquist plots (Figure 3e) indicated that the cathode contributed much more to the impedance than the anode. The cathode impedance increased from ≈55 to 75 Ω. The anode impedance was below 5 Ω for the first 10 cycles, and thus was challenging to be deconvoluted from the cathode.[47] However, the anode impedance was observed to increase as the cell operated, and hence could become possible to be deconvoluted from the cathode after 100 cycles. A similar EIS result was observed when the cell was fully discharged (Figure S8b, Supporting Information). The anode impedance increased to 10 Ω, but without obvious increase after 10 cycles. On the contrary, the cathode impedance, especially the charge transfer impedance (the semicircle with the lowest frequency[48]), increased significantly after 10 cycles (from ≈50 to 75 Ω). Thus, the smaller semicircle was assigned to anode. It is worthy to note that the anode potential in Figure S8c (Supporting Information)

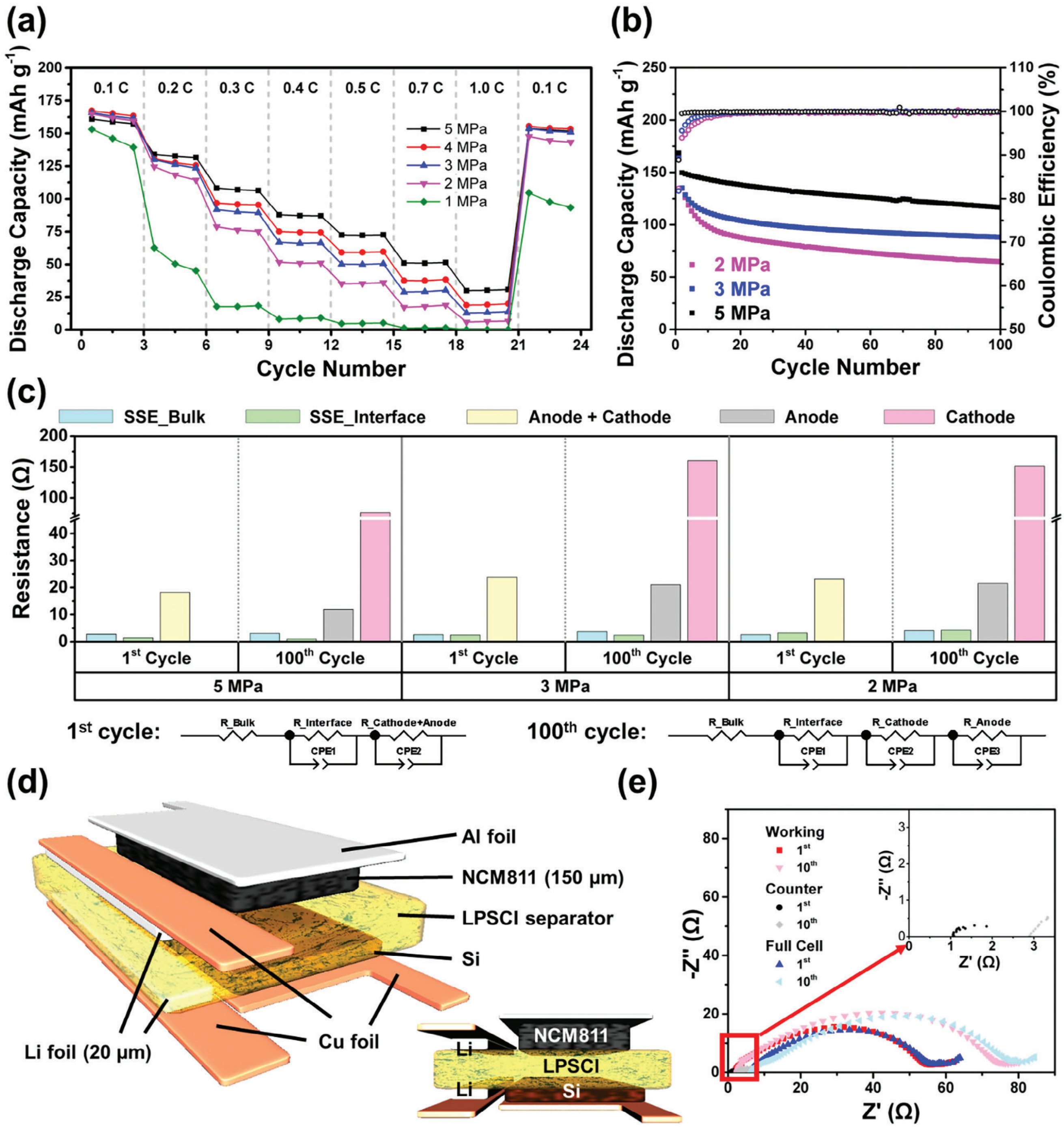

Figure 3. a) Rate capability test of pouch cells with different cycling pressures at different current densities. b) The capacity retention and Coulombic efficiency plots of pouch cells fabricated at 500 MPa and cycled at 5, 3, and 2 MPa. c) The EIS fitting results of the pouch cells measured after 1st and 100th cycle at 50% state of charge. d) The schematic of the structure of a three-electrode ASSPC. e) The Nyquist plots of cathode – Li (working), anode – Li (counter) and full cell (anode – cathode) EIS at 50% state of charge in 1st and 10th discharge.

is ≈250 to 500 mV versus Li/Li^+, which is the redox potential of Si,[11,47,49–52] indicates that the small anode impedance did not originate from short-circuiting between the anode and the reference electrodes. After charging the ASSPC to 4.3 V, the voltage of the cathode reached 4.45 V versus Li / Li^+ (Figure S8c, Supporting Information). Such a high cut-off voltage could lead to decreased structure stability for layered-oxide cathodes, and thus reduced capacity retention.[53,54] At the end of the discharge, both NCM811 and Si exhibited a steep voltage change, indicating that an N/P ratio of 1.2 is suitable for the system employed in this study, as the voltages of both the anode and the cathode changed rapidly by the end of discharge, which indicated both had reached their practical discharge capacity simultaneously. To further separate the degradation resulting from interfaces and bulk electrode materials, the galvanostatic intermittent titration technique (GITT) after the 1st and the 10th cycle was employed to probe the Li^+ diffusion coefficients (Figure S8d–g, Supporting Information). While there was no significant change on the Si anode, the Li^+ diffusion coefficients decreased drastically on the cathode (from ≈10^{-10} to 10^{-11} cm^2 S^{-1}). This indicates that polycrystal NCM811 might have cracking within their secondary particle, or spinel formation.[48,55] The success of the three-electrode ASSPC also highlighted the ability of IPCH to apply uniform pressure to uneven surfaces, as the thickness of Li, Si and NCM811 electrodes were not identical. When the cycling pressure decreased from 5 to 3 and 2 MPa, both cathode and anode impedance approximately doubled. This indicates that lower cycling pressures resulted in more loss in the physical contacts and such loss accumulated as it cycles. Consequently, it led to increased polarization and more capacity fading.

For practical use, isostatic ASSPC modules may occasionally need to be depressurized during idling, and the effect of depressurizing on electrochemical performance needs to be evaluated. To probe the impedance evolution of ASSPCs under pressure change when it is not in operation, an ASSPC after 100 cycles was put to idle and subjected to a pressure decrease from 5 to 1 MPa, re-pressurized back to 5 MPa, re-calendered at 500 MPa, and the EIS of each step was measured (the detailed procedure is described in Chart S1, Supporting Information). The EIS results are presented in **Figure 4**a, Figure S9 and Table S2 (Supporting Information). As the pressure decreased, the impedance of the cell gradually increased. While the impedance of the SSE separator layer increased by 1.7 times, both the interfacial impedance at the anode and the cathode increased ≈2.5 times when the pressure decreased from 5 to 1 MPa. The impedance of the ASSPC could not be restored even if the pressure resumed to 5 MPa. To restore the initial cell architecture, the ASSPC was re-calendered at 500 MPa and the impedance dropped significantly. Consequently, Figure 4b shows that the re-calendered ASSPC exhibited a higher discharge capacity of 141.2 mAh g^{-1} than that before it was re-calendered (116.5 mAh g^{-1}). To further validate the impact of re-calendering, the ASSPC that underwent the rate capability test at 1 MPa was subjected to re-calendering and then cycled again at 5 MPa. The performance was also almost fully restored, similar to the ASSPC cycled at 5 MPa from the beginning (Figure 4c; Figure S10, Supporting Information). The impedance change suggests that there is a microstructure evolution in the cathode composite as a function of the applied pressure (Figure 4d). When the applied pressure decreases, both the SSE and cathode particles can undergo volume relaxation to their low-pressure state even if the state of charge of the cell remains unchanged. This creates larger gaps, resulting in poor interfacial contact, and thus increases the cell impedance. As the friction between particles needs to be mitigated to eliminate gaps, high calendering pressure is required to reform the physical contact. It is worthy to note that the impedance could not be fully restored, as SEI and cathode electrolyte interface (CEI) had formed after long cycling.[56]

To validate the feasibility of a multi-layer pouch cell in IPCHs, a bilayer ASSPC (Cu | Si | SSE | NCM811 | Al | NCM811 | SSE | Si | Cu) with a total cathode area of 21 cm^2 and an areal theoretical capacity of ≈5 mAh cm^{-2} (which led to a total theoretical capacity of over 100 mAh) was assembled, and cycled at 5 MPa, 30 °C and 0.1 C. The FIB-SEM cross-sectional images and the details of the cell format are shown in **Figure 5**a,b. The bilayer ASSPC exhibited an initial Coulombic efficiency of 76.9% and discharge capacity of 173.6 mAh g^{-1} (88.1 mAh) which is close to the single layer pouch cell, indicating they have similar material utilization. After 100 cycles, a discharge capacity of 145.0 mAh g^{-1} was retained (Figure 5c,d). To examine the power capability of the bilayer ASSPC, it was used to power an incandescent light bulb with a rating of 2.5 V and 300 mA (Figure 5e), highlighting its ability to be discharged at 3 C. Although the current IPCH design might look bulky, its energy density can be further boosted by accommodating multiple ASSPCs in its chamber and improved module design.

3. Conclusion

As cycling pressure is required to maintain good interfacial contacts between different components in ASSBs, it is important to develop a pressurization system that enables uniform and accurate pressure to boost the electrochemical performance of ASSBs. In this study, we developed an IPCH that employed compressed air to apply a more homogenously distributed pressure than that of UPCHs with rigid metal surfaces or flexible rubber gaskets. As fluids do not suffer from material fatigue like many solid elastic materials, the IPCH enabled a higher capacity retention of an ASSPC than that of a UPCH over 100 cycles crediting to its stable pressurization. The minimum required cycling pressure to cycle NCM811 | LPSCl | Si ASSPCs was found to be as low as 2 MPa to deliver acceptable electrochemical performances, even at 1 C. However, a higher pressure is still preferred to maintain the intimate contact during long-term cycling. Additionally, the NCM811 cathode composite was found to contribute the most to the overall cell impedance, and thus accentuated the importance of optimizing cathode composites for future research. A bilayer ASSPC cycled in an IPCH showed a practical capacity of ≈88.1 mAh at 0.1 C for 50 cycles. Moreover, the cell was capable of discharging at a rate of 3 C (300 mA) powering an incandescent light bulb. The concept of isostatic pressurization in this study not only provides a uniform and accurate pressurizing method to study the pressure effects on ASSPCs, but also endeavors on the commercialization of ASSBs.

4. Experimental Section

Fabrication of Electrolytes and SSE Separators: Dry-processed $LiNi_{0.8}Co_{0.1}Mn_{0.1}O_2$ (NCM811, LG Energy Solution) cathode composite, dry-processed Li_6PS_5Cl (LPSCl, NEI Corporation) SSE separator and slurry-processed Si anode were employed in ASSPCs. To fabricate NCM811 cathode composite, NCM811, LPSCl, vapor-grown carbon fiber (VGCF, Sigma–Aldrich), and polytetrafluoroethylene (PTFE) were mixed in a mortar and a pestle at a weight ratio of 66:31: 3:0.1 until a dough formed. The dough was then transferred to a hot roller (TMAXCN) set at 60 °C to fabricate films following the protocol described in the previous article.[57] Shear force was applied during mixing and rolling to fibrillate PTFE and strengthen the films.[57–60] A similar procedure was applied to fabricate LPSCl SSE separator, with a weight ratio of LPSCl: PTFE = 99.9: 0.1. The EIS comparison of pristine LPSCl pellet and dry-processed LPSCl SSE separator with 0.1% PTFE is shown in Figure S11 (Supporting Information). The ionic conductivity decreased slightly from 1.88 to

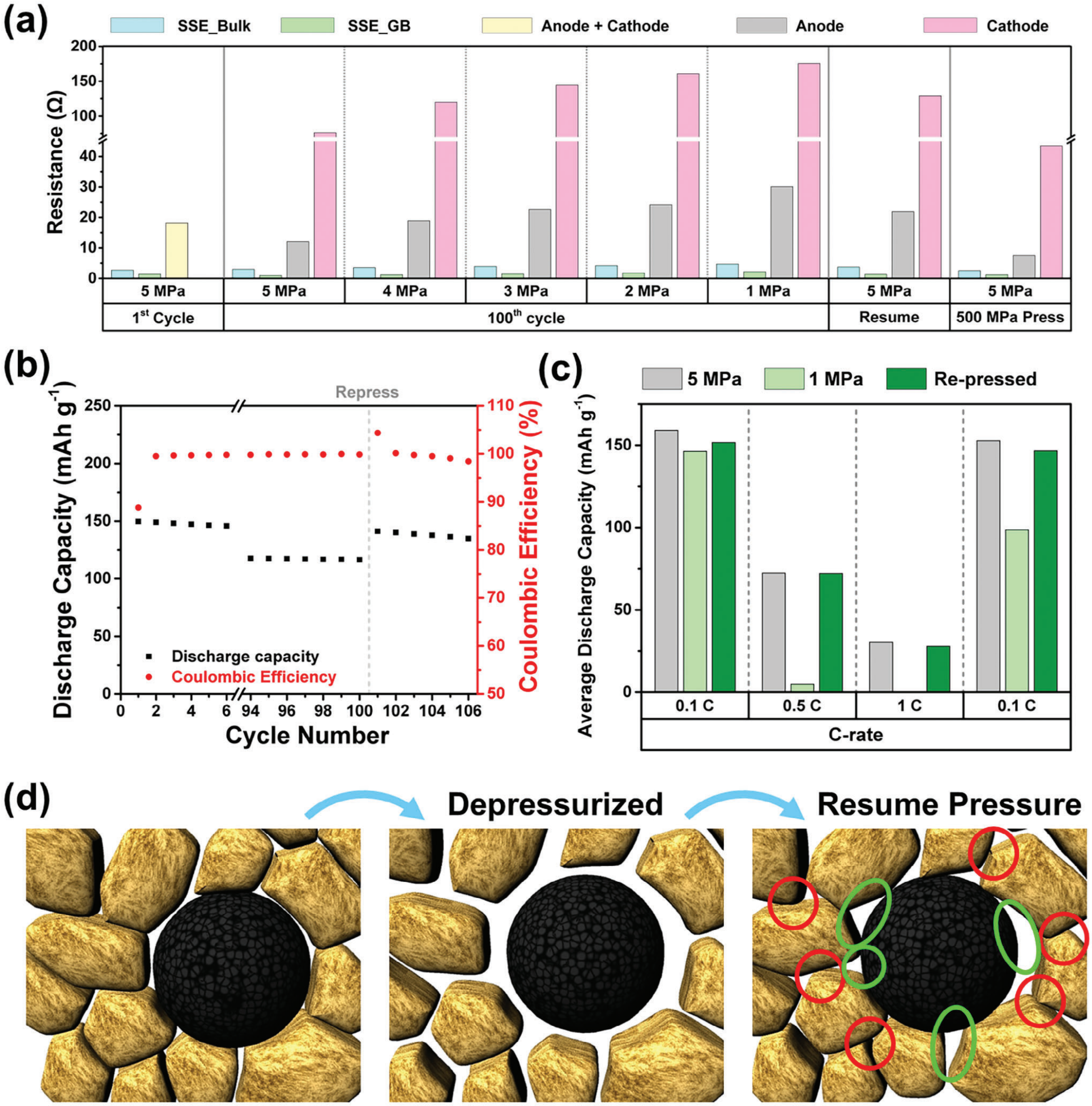

Figure 4. a) The EIS results of the ASSPC cycled at 5 MPa after 100 cycles, after decreasing the pressure to 1 MPa, resuming at 5 MPa, and then re-calendered at 500 MPa. b) the capacity retention and CE of the pouch cell cycled at 5 MPa before and after re-calendering. c) The average discharge capacity of the pouch cell having rate test at 1 MPa, re-calendering at 500 MPa, and having another rate test at 5 MPa. d) Schematic of the microstructure evolution between SSE and cathode when insufficient pressure is applied and the inability to restore to their original state even after the pressure returns to the initial value (red circles label the friction spots and green circles label the gaps). A much higher pressure must be applied to restore the contact between particles.

1.53 mS cm^{-1} after adding 0.1% PTFE. To prepare μ-Si electrodes, 99.9 wt.% μ-Si (Thermofisher) powder and 0.1 wt.% PVDF binder was dispersed in N-Methyl-2-Pyrrolidone (NMP) solvent using a Thinky mixer to create a slurry. The slurry was casted on a piece of 10 μm copper foil current collector using a doctor blade on an automatic film coater. The electrode was vacuum dried at 80 °C overnight to remove the solvent. The dried electrode was then punched into suitable shapes to be used for ASSPC fabrication.

Fabrication of ASSPCs: Three pouch cell formats were used in this study: two-electrode, three-electrode electrochemical characterization cells, and bilayer cells. Cathode composite films with a dimension of 15 mm × 35 mm × 160 μm (resulting in an areal loading of 4 mAh cm^{-2}),

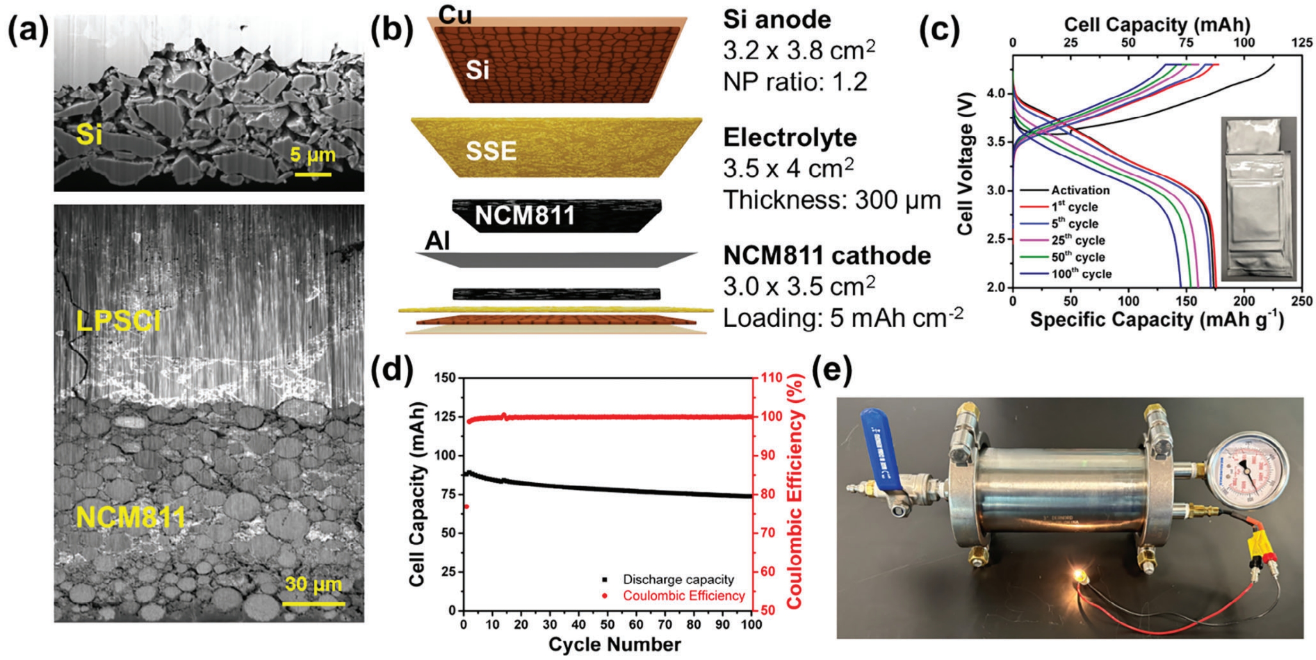

Figure 5. a) The P-FIB SEM cross-section and b) the schematic and illustrating the bilayer pouch cell configuration. The c) voltage profiles at different cycle numbers and d) capacity retention of the 3 × 3.5 cm^2 bilayer ASSPC. e) A bilayer ASSPC powering an incandescent light bulb with an input rating of 2.5 V–300 mA under5 MPa of isostatic cycling pressure.

SSE separators with a dimension of 20 mm × 50 mm × 300 µm, and Si anode with NP ratio of 1.2 and a dimension of 18 mm × 40 mm were selected for two-electrode electrochemical characterization cells. The NP ratio of 1.2 was selected because it was sufficiently high to prevent short circuiting, but also close enough to 1 to avoid decreasing the energy density and the initial coulombic efficiency (Figure S12, Supporting Information).[6,61] The area of the cathode composite films was the smallest, as it was selected as the capacity limiting component, and SSE separators were the largest to electronically separate cathodes and anodes. To assemble an electrochemical characterization cell, Cu, Si, LPSCl, NCM811 cathode composite and Al were stacked from bottom to top and secured with Kapton tape. An Al tab was welded to the Al current collector as the positive terminal, and a Ni tab to the Cu current collector as the negative terminal (both terminals were 4 mm in width). The whole stack was then vacuum sealed in the Al laminated film and calendered using a cold isostatic press (MTI Corporation). To understand the effect of calender pressure on the electrochemical performance, ASSPCs calendered at 150, 350 and 500 MPa with 3 min hold time were cycled and characterized (Figures S13 and S14 and Note S2, Supporting Information). 500 MPa was selected to calendar the ASSPCs to study the effect of cycling pressure, as it was the largest pressure that the equipment could provide and yielded the best electrochemical performance. After calendering, cycling pressures were applied to ASSPCs using UPCHs and IPCHs. All the bolts and nuts of the UPCHs were lubricated with grease to obtain low and consistent friction. When torquing the bare UPCH, a torque wrench was used to torque all four nuts sequentially and the torque value was gradually increased in each rotation to the target value to ensure parallelism of the metal plates. The target torque value was predetermined by monitoring the clamping force of an empty UPCH with a force sensor and the same torque value was applied to the later ASSPC tests. A high-pressure air compressor was used to apply cycling pressure for IPCHs. To fabricate three-electrode electrochemical characterization cells, the horizontal dimensions of cathodes and anodes were reduced to 10 mm × 35 mm and 12 mm × 40 mm. Two pieces of Li metal (20 µm thick, Honjo Chemical Cooperation) were placed next to the cathode and anode, and on both sides of the SSE separator (Figure 3d; Figure S8a, Supporting Information). The as assembled three-electrode cells were calendered only once at 150 MPa with a short hold time to prevent excessive Li-creeping. The rest of the fabrication steps were identical to those of two-electrode electrochemical characterization cells. Cathode composite films with a dimension of 30 mm × 35 mm × 200 µm (resulted in an areal loading of 5 mAh cm^{-2}), SSE separators with a thickness of 35 mm × 40 mm 300 µm, and Si anode with NP ratio of 1.2 and a dimension of 35 mm × 37 mm were selected for bilayer cells. They were stacked in a sequence of Cu, Si, LPSCl, NCM811 cathode composite, Al, NCM811 cathode composite, LPSCl, Si, and Cu. The rest of the fabrication steps were identical to those of electrochemical characterization cells.

Galvanostatic Cycling and Electrochemical Impedance Spectroscopy (EIS) of ASSPCs: Neware A211-BTS-4S-1U-100mA-124 battery cyclers and a Biologic VSP-300 were employed for galvanostatic cycling and EIS measurements. A voltage cutoff of 2 to 4.3 V was selected for NCM811 | Si system.[6] As Li diffusivity in pure Si could be improved only after lithiation,[6] an activation cycle was introduced in all testing protocols. In the activation cycle, ASSPCs were cycled at 0.05 C for 5 h, and then completed the whole cycle at 0.1 C. 5 MPa was chosen as the activation pressure for the activation cycle and later reduced to their target pressures to achieve lower polarization, smoother voltage profile and lower a chance of short circuiting (Figure S15, Supporting Information). To obtain accurate cycling data, all ASSPCs were cycled in an oven set at 30 °C to study the effect of cycling pressure. The rate capability test was conducted by running the ASSPCs at 0.1, 0.2, 0.3, 0.4, 0.5, 0.7, 1, and 0.1 C and each C-rate for 3 cycles under 5 to 1 MPa. In the long-term cycling test, ASSPCs were cycled at 0.2 C and a constant voltage step till 0.05 C was applied at the end of charging. The ASSPCs were cycled for 100 cycles and EIS was obtained in the 1st and 100th cycle at 50% state of charge during discharge. Z-View software was used to analyze EIS results. The EIS of the three-electrode ASSPC was recorded at the ambient temperature in the 1st and the 10th cycle at state of charge of 50% and 0% during discharge. The galvanostatic intermittent titration technique (GITT) of the three-electrode ASSPC was conducted after the activation cycle and the 10th cycle by applying a pulse current at 0.1 C with a duration of 10 min and followed by

60 min pause time. NCM811 cathode, Si anode and Li metal electrode were connected to working, counter and reference electrodes. Afterward, the three-electrode ASSPC was cycled using Biologic VSP-300 at ambient temperature to record the voltage profiles of cathode – Li, anode – Li and full cell. The bilayer ASSPC was cycled at 0.1 C and a constant voltage step till 0.05 C was applied at the end of charging.

Characterization and Image Processing: A Helios G4 PFIB UXe DualBeam plasma focused ion beam/scanning electron microscope (P-FIB/SEM) with a xenon source was used to obtain the cross section of ASSPCs. After the ASSPCs were calendered, they were disassembled, and their cathode composites were attached to SEM stubs and sealed in an Ar-filled glovebox. The stubs were then transferred to P-FIB/SEM within 30 s of air exposure. Sample milling was conducted at 30 kV with a 2.5 µA current. Afterward, a lower current (500 and 60 nA) was used to polish the cross-section. Electron imaging was conducted at 5 kV and 4 nA beam conditions. To segment the P-FIB/SEM images, they were imported into the Trainable Weka Segmentation Fiji module[62] to identify NMC811, LPSCl and pores. The segmentation relies on machine-learning algorithms that were manually trained by the user with the input images. The phase ratios were then computed in MATLAB. The images of pressure paper were also processed: based on pictures of the pressure papers, the results were rescaled in MATLAB using the ratio between the red color and the green and blue colors for each pixel in the jpg files.

Supporting Information

Supporting Information is available from the Wiley Online Library or from the author.

Acknowledgements

Y.-T.C. and J.J. contributed equally to this work. This work was partially supported by LG Energy Solution through the Frontier Research Laboratory (FRL) program. Part of this work was performed at the San Diego Nanotechnology Infrastructure (SDNI) of the UCSD, a member of the National Nanotechnology Coordinated Infrastructure, supported by the National Science Foundation (Grant ECCS-1542148). The authors acknowledge the use of facilities and instrumentation at the UC Irvine Materials Research Institute (IMRI) supported in part by the National Science Foundation Materials Research Science and Engineering Center program through the UC Irvine Center for Complex and Active Materials (DMR-2011967). The authors also acknowledge the support from Coherent/II-VI Foundation.

Conflict of interest

Two joint patent applications on this work have been filed (US 63/546685 and US 63/547809) between UC San Diego's Office of Innovation and Commercialization as well as LG Energy Solution, Ltd.

Data Availability Statement

The data that support the findings of this study are available from the corresponding author upon reasonable request.

Keywords

All-solid-state batteries, isostatic cycling pressure, pouch cells

Received: December 14, 2023
Revised: April 16, 2024
Published online:

[1] Y. Horowitz, C. Schmidt, D.-h. Yoon, L. M. Riegger, L. Katzenmeier, G. M. Bosch, M. Noked, Y. Ein-Eli, J. Janek, W. G. Zeier, *Energy Technol.* **2020**, *8*, 2000580.
[2] Y. S. Jung, D. Y. Oh, Y. J. Nam, K. H. Park, *Isr. J. Chem.* **2015**, *55*, 472.
[3] K. Kerman, A. Luntz, V. Viswanathan, Y.-M. Chiang, Z. Chen, *J. Electrochem. Soc.* **2017**, *164*, A1731.
[4] H. Lee, P. Oh, J. Kim, H. Cha, S. Chae, S. Lee, J. Cho, *Adv. Mater.* **2019**, *31*, 1900376.
[5] S. Cangaz, F. Hippauf, F. S. Reuter, S. Doerfler, T. Abendroth, H. Althues, S. Kaskel, *Adv. Energy Mater.* **2020**, *10*, 2001320.
[6] D. H. Tan, Y.-T. Chen, H. Yang, W. Bao, B. Sreenarayanan, J.-M. Doux, W. Li, B. Lu, S.-Y. Ham, B. Sayahpour, *Science* **2021**, *373*, 1494.
[7] C. K. Chan, H. Peng, G. Liu, K. McIlwrath, X. F. Zhang, R. A. Huggins, Y. Cui, *Nat. Nanotechnol.* **2008**, *3*, 31.
[8] H. Wu, G. Chan, J. W. Choi, I. Ryu, Y. Yao, M. T. McDowell, S. W. Lee, A. Jackson, Y. Yang, L. Hu, *Nat. Nanotechnol.* **2012**, *7*, 310.
[9] N. Liu, Z. Lu, J. Zhao, M. T. McDowell, H.-W. Lee, W. Zhao, Y. Cui, *Nat. Nanotechnol.* **2014**, *9*, 187.
[10] L.-F. Cui, R. Ruffo, C. K. Chan, H. Peng, Y. Cui, *Nano Lett.* **2009**, *9*, 491.
[11] X. Su, Q. Wu, J. Li, X. Xiao, A. Lott, W. Lu, B. W. Sheldon, J. Wu, *Adv. Energy Mater.* **2014**, *4*, 1300882.
[12] A. Banerjee, X. Wang, C. Fang, E. A. Wu, Y. S. Meng, *Chem. Rev.* **2020**, *120*, 6878.
[13] R. Koerver, I. Aygün, T. Leichtweiß, C. Dietrich, W. Zhang, J. O. Binder, P. Hartmann, W. G. Zeier, J. r. Janek, *Chem. Mater.* **2017**, *29*, 5574.
[14] T. Shi, Y.-Q. Zhang, Q. Tu, Y. Wang, M. Scott, G. Ceder, *J. Mater. Chem. A* **2020**, *8*, 17399.
[15] Y.-T. Chen, M. Duquesnoy, D. H. Tan, J.-M. Doux, H. Yang, G. Deysher, P. Ridley, A. A. Franco, Y. S. Meng, Z. Chen, *ACS Energy Lett.* **2021**, *6*, 1639.
[16] D. H. Tan, Y. S. Meng, J. Jang, *Joule* **2022**, *6*, 1755.
[17] S. Liu, L. Zhou, J. Han, K. Wen, S. Guan, C. Xue, Z. Zhang, B. Xu, Y. Lin, Y. Shen, *Adv. Energy Mater.* **2022**, *12*, 2200660.
[18] C. Wang, J. T. Kim, C. Wang, X. Sun, *Adv. Mater.* **2023**, *35*, 2209074.
[19] M. Dixit, C. Beamer, R. Amin, J. Shipley, R. Eklund, N. Muralidharan, L. Lindqvist, A. Fritz, R. Essehli, M. Balasubramanian, *ACS Energy Lett.* **2022**, *7*, 3936.
[20] Y. Sakka, H. Yamashige, A. Watanabe, A. Takeuchi, M. Uesugi, K. Uesugi, Y. Orikasa, *J. Mater. Chem. A* **2022**, *10*, 16602.
[21] Y.-G. Lee, S. Fujiki, C. Jung, N. Suzuki, N. Yashiro, R. Omoda, D.-S. Ko, T. Shiratsuchi, T. Sugimoto, S. Ryu, *Nat. Energy* **2020**, *5*, 299.
[22] K. Fu, Y. Gong, B. Liu, Y. Zhu, S. Xu, Y. Yao, W. Luo, C. Wang, S. D. Lacey, J. Dai, *Sci. Adv.* **2017**, *3*, e1601659.
[23] K. Fu, Y. Gong, J. Dai, A. Gong, X. Han, Y. Yao, C. Wang, Y. Wang, Y. Chen, C. Yan, *Proc. Natl. Acad. Sci. USA* **2016**, *113*, 7094.
[24] H. S. Shin, W. G. Ryu, M. S. Park, K. N. Jung, H. Kim, J. W. Lee, *ChemSusChem* **2018**, *11*, 3184.
[25] G. T. Hitz, D. W. McOwen, L. Zhang, Z. Ma, Z. Fu, Y. Wen, Y. Gong, J. Dai, T. R. Hamann, L. Hu, *Mater. Today* **2019**, *22*, 50.
[26] X. Zhang, T. Liu, S. Zhang, X. Huang, B. Xu, Y. Lin, B. Xu, L. Li, C.-W. Nan, Y. Shen, *J. Am. Chem. Soc.* **2017**, *139*, 13779.
[27] C. Wang, Q. Sun, Y. Liu, Y. Zhao, X. Li, X. Lin, M. N. Banis, M. Li, W. Li, K. R. Adair, *Nano Energy* **2018**, *48*, 35.
[28] E. Yi, H. Shen, S. Heywood, J. Alvarado, D. Y. Parkinson, G. Chen, S. W. Sofie, M. M. Doeff, *ACS Appl. Energy Mater.* **2020**, *3*, 170.
[29] W. Luo, Y. Gong, Y. Zhu, Y. Li, Y. Yao, Y. Zhang, K. Fu, G. Pastel, C. F. Lin, Y. Mo, *Adv. Mater.* **2017**, *29*, 1606042.
[30] Y. Shao, H. Wang, Z. Gong, D. Wang, B. Zheng, J. Zhu, Y. Lu, Y.-S. Hu, X. Guo, H. Li, *ACS Energy Lett.* **2018**, *3*, 1212.
[31] F. Zhang, Y. Guo, L. Zhang, P. Jia, X. Liu, P. Qiu, H. Zhang, J. Huang, *Etransportation* **2022**, *15*, 100220.

[32] R. Koerver, W. Zhang, L. de Biasi, S. Schweidler, A. O. Kondrakov, S. Kolling, T. Brezesinski, P. Hartmann, W. G. Zeier, J. Janek, *Energy Environ. Sci.* **2018**, *11*, 2142.
[33] S.-Y. Ham, H. Yang, O. Nunez-cuacuas, D. H. Tan, Y.-T. Chen, G. Deysher, A. Cronk, P. Ridley, J.-M. Doux, E. A. Wu, *Energy Storage Mater.* **2023**, *55*, 455.
[34] D. Lin, Y. Liu, Y. Cui, *Nat. Nanotechnol.* **2017**, *12*, 194.
[35] S. Ito, S. Fujiki, T. Yamada, Y. Aihara, Y. Park, T. Y. Kim, S.-W. Baek, J.-M. Lee, S. Doo, N. Machida, *J. Power Sources* **2014**, *248*, 943.
[36] A. Sakuda, K. Kuratani, M. Yamamoto, M. Takahashi, T. Takeuchi, H. Kobayashi, *J. Electrochem. Soc.* **2017**, *164*, A2474.
[37] Y. J. Nam, D. Y. Oh, S. H. Jung, Y. S. Jung, *J. Power Sources* **2018**, *375*, 93.
[38] H. Yuan, H. X. Nan, C. Z. Zhao, G. L. Zhu, Y. Lu, X. B. Cheng, Q. B. Liu, C. X. He, J. Q. Huang, Q. Zhang, *Batter. Supercaps* **2020**, *3*, 596.
[39] M. Fiedler, S. Cangaz, F. Hippauf, S. Dörfler, T. Abendroth, H. Althues, S. Kaskel, *Adv. Sustain. Syst.* **2023**, *7*, 2200439.
[40] J. Li, Y. Li, S. Zhang, T. Liu, D. Li, L. Ci, *Chem. Eng. J.* **2023**, *455*, 140605.
[41] J. Kim, M. J. Kim, J. Kim, J. W. Lee, J. Park, S. E. Wang, S. Lee, Y. C. Kang, U. Paik, D. S. Jung, *Adv. Funct. Mater.* **2023**, *33*, 2211355.
[42] Y. S. Park, K. Kim, J. W. Lee, J. W. Moon, H. H. Park, H. Hwang, *J. Am. Ceram. Soc.* **2023**, *106*, 7322.
[43] Z. Zhang, S. Chen, J. Yang, J. Wang, L. Yao, X. Yao, P. Cui, X. Xu, *ACS Appl. Mater. Interfaces* **2018**, *10*, 2556.
[44] D. Cao, X. Sun, Y. Li, A. Anderson, W. Lu, H. Zhu, *Adv. Mater.* **2022**, *34*, 2200401.
[45] S. Hori, R. Kanno, X. Sun, S. Song, M. Hirayama, B. Hauck, M. Dippon, S. Dierickx, E. Ivers-Tiffée, *J. Power Sources* **2023**, *556*, 232450.
[46] S. J. An, J. Li, C. Daniel, S. Kalnaus, D. L. Wood, *J. Electrochem. Soc.* **2017**, *164*, A1755.
[47] S. Poetke, S. Cangaz, F. Hippauf, S. Haufe, S. Dörfler, H. Althues, S. Kaskel, *Energy Technol.* **2023**, *11*, 2201330.
[48] J. Zheng, W. Shi, M. Gu, J. Xiao, P. Zuo, C. Wang, J.-G. Zhang, *J. Electrochem. Soc.* **2013**, *160*, A2212.
[49] X. Li, M. Zhang, S. Yuan, C. Lu, *ChemElectroChem* **2020**, *7*, 4289.
[50] J.-Y. Li, Q. Xu, G. Li, Y.-X. Yin, L.-J. Wan, Y.-G. Guo, *Mater. Chem. Front.* **2017**, *1*, 1691.
[51] H. Liu, Q. Sun, H. Zhang, J. Cheng, Y. Li, Z. Zeng, S. Zhang, X. Xu, F. Ji, D. Li, *Energy Storage Mater.* **2022**, *55*, 244.
[52] X. Zuo, J. Zhu, P. Müller-Buschbaum, Y.-J. Cheng, *Nano Energy* **2017**, *31*, 113.
[53] S. K. Jung, H. Gwon, J. Hong, K. Y. Park, D. H. Seo, H. Kim, J. Hyun, W. Yang, K. Kang, *Adv. Energy Mater.* **2014**, *4*, 1300787.
[54] J. Choi, A. Manthiram, *J. Electrochem. Soc.* **2005**, *152*, A1714.
[55] H.-H. Ryu, B. Namkoong, J.-H. Kim, I. Belharouak, C. S. Yoon, Y.-K. Sun, *ACS Energy Lett.* **2021**, *6*, 2726.
[56] D. H. Tan, E. A. Wu, H. Nguyen, Z. Chen, M. A. Marple, J.-M. Doux, X. Wang, H. Yang, A. Banerjee, Y. S. Meng, *ACS Energy Lett.* **2019**, *4*, 2418.
[57] D. J. Lee, J. Jang, J. P. Lee, J. Wu, Y. T. Chen, J. Holoubek, K. Yu, S. Y. Ham, Y. Jeon, T. H. Kim, *Adv. Funct. Mater.* **2023**, *33*, 2301341.
[58] C. Wang, R. Yu, H. Duan, Q. Lu, Q. Li, K. R. Adair, D. Bao, Y. Liu, R. Yang, J. Wang, *ACS Energy Lett.* **2021**, *7*, 410.
[59] Y. Li, Y. Wu, Z. Wang, J. Xu, T. Ma, L. Chen, H. Li, F. Wu, *Mater. Today* **2022**, *55*, 92.
[60] F. Hippauf, B. Schumm, S. Doerfler, H. Althues, S. Fujiki, T. Shiratsuchi, T. Tsujimura, Y. Aihara, S. Kaskel, *Energy Storage Mater.* **2019**, *21*, 390.
[61] S.-Y. Ham, E. Sebti, A. Cronk, T. Pennebaker, G. Deysher, Y.-T. Chen, J. A. S. Oh, J. B. Lee, M. S. Song, P. Ridley, *Nat. Commun.* **2024**, *15*, 2991.
[62] I. Arganda-Carreras, V. Kaynig, C. Rueden, K. W. Eliceiri, J. Schindelin, A. Cardona, H. Sebastian Seung, *Bioinformatics* **2017**, *33*, 2424.